Thermal Lens Spectroscopy in Liquid Argon Solutions: ($\Delta v = 6$) C−H Vibrational Overtone Absorption of Methane†

Juan G. Navea, Alfredo Lopez-Calvo, and Carlos E. Manzanares*

Department of Chemistry & Biochemistry, Baylor University, 101 Bagby Avenue, Baylor Sciences Building E-216, Waco, Texas 76798

Received: July 15, 2005; In Final Form: September 19, 2005

A dual-beam thermal lens technique has been used to obtain the absorption spectrum of the ($\Delta v = 6$) C−H stretch of liquid methane and methane in liquid argon solutions. The lowest concentration detected was 1×10^{-3} (mole fraction) of CH_4 in liquid Ar with a continuous wave laser power of 20 mW. The thermal lens signal is linear with the mole fraction of methane up to 1×10^{-2} but not for higher concentrations. Considering the system CH_4−Ar as an ideal solution, the factors that contribute to the thermal lens signal were calculated as a function of the concentration of methane. A mechanism of energy transfer based on the gas-phase results could explain qualitatively the dependence of the magnitude of the signal on the mole fraction of methane.

1. Introduction

Use of the thermal lens technique to study vibrational overtone absorptions in liquids has its origin in the work of Long, Swofford, and Albrecht.[1] Vibrational overtone ($\Delta v = 5-7$) absorptions of C−H and O−H bonds have been measured by Swofford et al.[2,3] and Fang and Swofford [4,5] at room temperature. Thermal lens spectroscopy (TLS) is a sensitive technique which relies on measurement of thermal changes induced by absorption of energy from a laser beam passing through a liquid or solid sample.[6−12] In TLS an absorbing sample is excited by a pump beam producing significant heating along the optical path. This heating is the result of nonradiative relaxation of excited molecules. The heating creates in the liquid a transverse temperature distribution that is cylindrically symmetric. If the mode of the beam is TEM_{00}, a radial Gaussian intensity profile is produced. With the aim of reaching thermodynamic equilibrium, natural thermal diffusion of the solvent occurs with an analogous change of its refraction index. Since most liquids show a positive coefficient of thermal expansion, the temperature coefficient of the index of refraction is negative, producing a divergent thermal lens. In the dual-beam configuration a second beam called "probe laser" is directed along the same path as the pump beam; consequently, the probe beam passes through a change in the optical path equivalent to the magnitude of the probe beam divergence. The magnitude of the divergence is proportional to the magnitude of the absorption by the sample.

The thermal lens signal has been shown to be a function of the excitation laser power and the thermooptical characteristics of the solvent.[12] Solvents that allow the absorbing sample to dissipate the excitation energy (electronic (E), vibrational (V), or rotational (R)) more efficiently into translational (T) energy are expected to increase the sensitivity of the technique. To our knowledge, the thermal lens technique has not been used to observe E, V, or R transitions of molecules in solution with liquefied monatomic gases as solvents. Use of liquefied gases (He, Ne, Ar, Kr, and Xe) as solvents should, in principle, provide an increase in the sensitivity of the technique due to the fact that the only possible energy-transfer mechanism is the conversion of internal energy (EVR, VR, or R) from the sample to translational energy of the monatomic solvent. Also, the low temperature of the cryogenic solvent should give a larger temperature gradient compared to a sample in a solution at room temperature.

Another motivation for this work is that the thermal lens experiments in the literature usually involve very dilute solutions where the laser wavelength is tuned to an electronic transition of the solute with a large absorption coefficient (α). Under these conditions the thermal properties ($-dn/dT$) and κ are associated with properties of the solvent. By exciting a high vibrational overtone, the absorption coefficient of the sample is always very small. This means that in our experiment we will be able to observe the thermal lens signal over the total range of concentrations of the solute. In this case the thermal properties of the solution (not the solvent) are the ones to be explored.

In this paper we used the dual-beam thermal lens technique to study an overtone absorption of methane in liquid argon solutions. Previously we measured this transition with an acoustic method, producing excitation of the molecules with a cw dye laser and detecting the absorption with a piezoelectric disk.[13,14] Almost identical thermophysical properties of the solution enhance the photoacoustic and thermal lens signals.[12,15] This study allows us to compare the flexibility of the two techniques. The thermal lens signals obtained are discussed in terms of properties of the solution such as thermal conductivity (κ), density (ρ), coefficient of thermal expansion (β), and negative temperature gradient of the index of refraction ($-dn/dT$). The mechanism of energy transfer and its influence on the thermal lens signal are also discussed.

2. Experimental Section

The experimental set up is shown in Figure 1. An argon ion laser (Spectra Physics 2017) operating at a wavelength of 488 nm and laser power of 3.5 W is used to pump a continuous wave dye laser. The tunable dye laser (Coherent CR-599) is scanned in the range of the laser dye (Kiton red) from 602 to 650 nm. A chopper is used to modulate the dye laser beam at

† Part of the special issue "William Hase Festschrift".

* Corresponding author. E-mail: Carlos_Manzanares@baylor.edu.

10.1021/jp053900g CCC: $33.50
Published on Web 10/22/2005

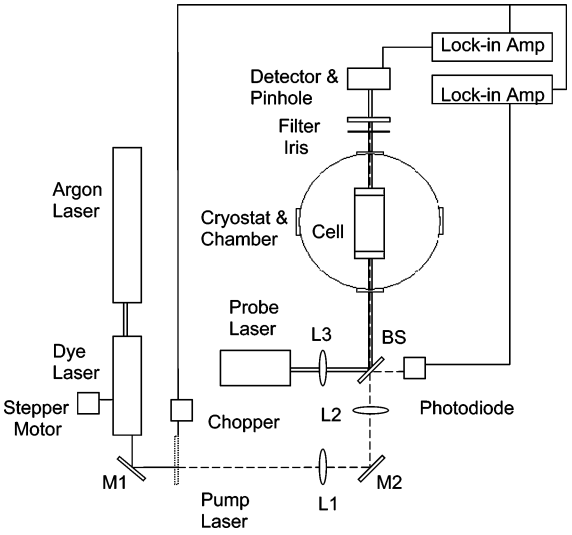

Figure 1. Experimental set up for the dual-beam thermal lens technique at cryogenic temperatures.

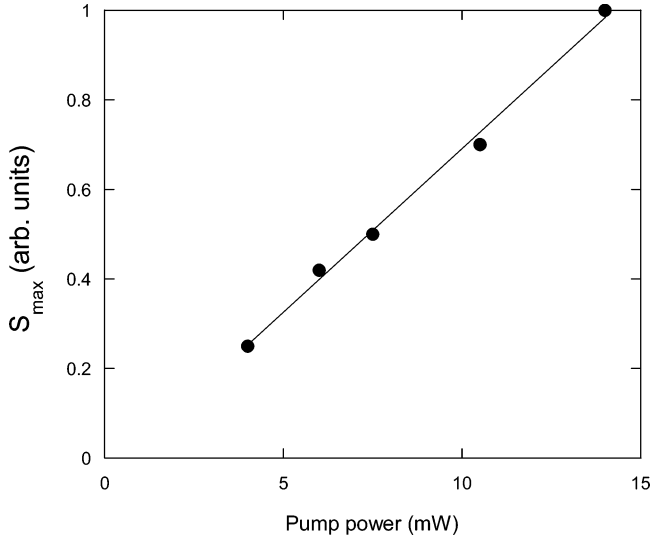

Figure 2. Normalized thermal lens signal (S_{max}) as a function of the power of the pump laser. The probe laser power is 6 mW, and the mole fraction of CH_4 in liquid Ar is $x_2 = 0.044$.

10 Hz. Wavelength tuning of the dye laser (1 cm^{-1} bandwidth) is accomplished with a stepper motor. The dye laser is used as the sample heating beam or pump beam. A second beam of an argon ion laser operating at 488 nm and a power of 6 mW was employed as the probe beam. The two beams come together at a beam splitter and travel collinearly through the sample cell inside a cryostat. At the center of the cell the radius of the pump beam is 0.030 cm and the radius of the probe beam is 0.091 cm. The confocal lengths are 51 (pump) and 0.87 cm (probe). The length of the sample cell is 10 cm. The radius of the pump beam does not change significantly throughout the cell due to the confocal length being 51 cm. The radius of the probe beam is 0.062 cm at the cell entrance and 0.116 cm at the cell exit. The divergence of the transmitted probe beam is monitored by measuring intensity changes at its center. The probe beam passes through an interference filter that transmits the 488 nm wavelength and blocks the dye laser pump beam. The residual transmission of the pump beam is filtered out by means of a blue filter placed in front of the detector. After passing through a 20 μm diameter pinhole the probe beam is detected with a photodiode. The signal from the detector is preamplified and directed to a lock-in amplifier. Simultaneously, a fraction of the dye laser beam (reflected at the beam splitter) is detected by another combination of photodiode and lock-in amplifier. Normalization of the thermal lens signal is achieved by dividing the output voltages of both lock-in amplifiers. Using LabView software a computer controls the dye laser wavelength scan, digitalizing and storing the normalized signal as a function of the wavelength.

The cryostat consists of a cylindrical aluminum vacuum chamber 180 mm in length and 110 mm in external diameter with four quartz windows symmetrically placed. Each window is 25.4 mm in diameter and 6.35 mm thick. Thermal isolation is achieved by having the chamber evacuated at pressures below 10^{-4} Torr. The cell is a copper (OFHC) cylinder 25 mm in external diameter, 12 mm in internal diameter, and 100 mm in length. It has sapphire windows at each end that are 2 mm thick and 20 mm in diameter. The birefringence of the sapphire windows was tested by passing a laser beam through the windows at different orientations with respect to each other. There was no significant change of the power of the laser. The interface cell-window is sealed with indium O rings, and the windows are fastened to the cell with flat circular flanges. The cell is firmly attached to the cold head in the cryostat. To introduce the sample the cell is connected to an external gas handling system through a short piece of stainless steel tubing 3.17 mm in diameter and 120 mm in length. The cell temperature is controlled by a Scientific Instruments model SI-9650 temperature controller with the following specifications: accuracy $\pm$0.1 (1.5−25 K) and $\pm$0.5 K (25−450 K), controllability $\pm$0.1 (1.5−25 K) and $\pm$0.2 K (25−450 K), repeatability $\pm$0.1 K, and resolution 0.01 K. The temperature is measured with two silicon diode sensors (model SI-410), one attached to the cell and the other attached to the cryostat head. Temperature readout is provided by the same controller.

3. Results

The experimental set up has been used to detect a high vibrational level of pure liquefied methane and samples of methane in liquid argon solutions. To show that the signal is linear as a function of the combined power of the pump and probe lasers, two different experiments were done. For the first experiment the sample was pure liquid ethane at 100 K. The pump laser power at $\lambda = 635$ nm (15 748 cm^{-1}) was changed between 8 and 55 mW with the probe laser at constant power of 6 mW. The second experiment was done with a CH_4−Ar solution. The mole fraction of methane was 0.044, and the pump laser power at $\lambda = 621.9$ nm (16 080 cm^{-1}) was changed between 4 and 14 mW with the probe laser at constant power of 6 mW. In both experiments the photothermal signal was linear as a function of the power of the pump laser. The results of the second experiment are shown in Figure 2.

A plot of the thermal lens signal as a function of wavenumber for liquid methane at 93 K is shown in Figure 3. Deconvolution of the spectrum shows two bands that have been previously reported.[13] In normal mode notation they are assigned to the main overtone transition ($5\nu_1 + \nu_3$) and the combination band ($4\nu_1 + \nu_3 + 2\nu_4$). The main peak is located at 16 080 cm^{-1} and has a full-width at half-maximum (fwhm) value of 213 cm^{-1}. These results are in excellent agreement with the absorption band reported previously using the cw photoacoustic technique.[13] The absorption band has a similar shape with a peak absorption at 16 075 cm^{-1} and fwhm of 225 cm^{-1}.

The thermal lens spectra of the diluted solutions of methane in liquid argon are shown in Figure 4. The smallest mole fraction of methane detected was $x_2 = 1 \times 10^{-3}$. The magnitude of the

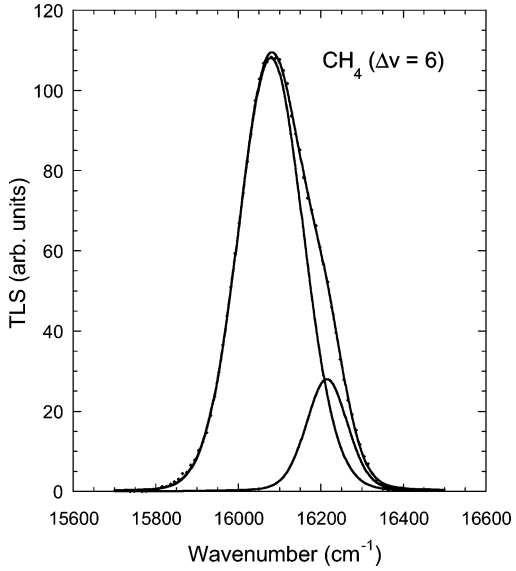

Figure 3. Deconvoluted thermal lens signal corresponding to the C−H ($\Delta v = 6$) absorption versus wavenumber for liquid methane at 93 K.

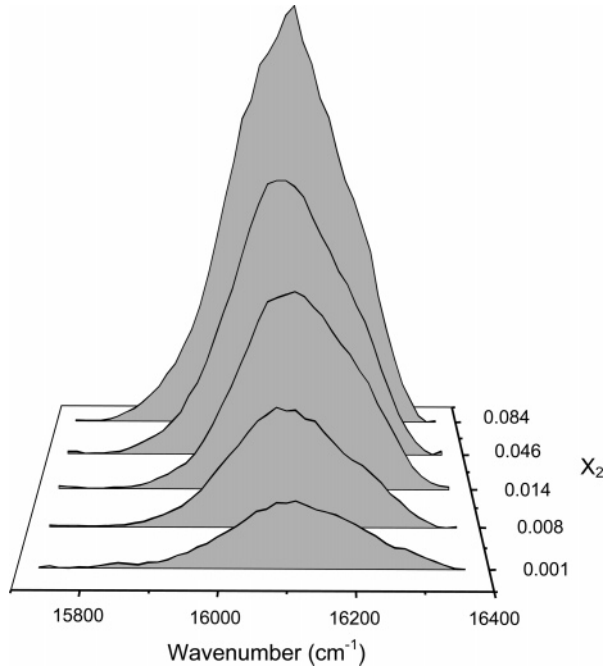

Figure 4. Thermal lens signal corresponding to the C−H ($v = 6$) absorption as a function of the wavenumber and mole fraction of methane in liquid argon at 93 K. The signal of the smallest mole fraction (0.001) has been multiplied by 5.

maximum value of the thermal lens signal (S_{max}) is presented as a function of the mole fraction of methane ($x_2 = 0-0.1$) in Figure 5 (top). Empirically we determined that the signal at the peak absorption (S_{max}) seems to be linear with the square root of the mole fraction $(x_2)^{1/2}$ over the range of mole fractions from 0 to 0.1. Figure 5 (bottom) shows S_{max} as a function of $(x_2)^{1/2}$. The square of the signal $(S_{max})^2$ is proportional to the mole fraction (x_2). The linear dependence of $(S_{max})^2$ vs (x_2) cannot be attributed to nonlinear effects such as two-photon absorption because, as shown in Figure 2, the probe laser signal is linear with the pump laser power.

4. Discussion

4.1. Thermal Lens Signal. The dual-laser (cw) photothermal technique is based on using one laser (pump) to create the thermal lens and a second laser (probe) to observe the time evolution of the thermal lens. With the pinhole aperture placed far from the sample cell and with the pump and probe lasers focused at distances, z and z', respectively, in front of the sample cell, the thermal lens signal is[12]

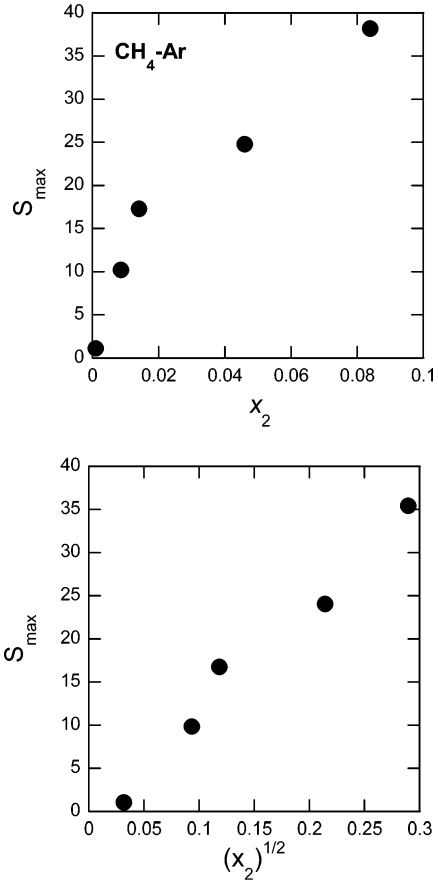

Figure 5. (Top) Thermal lens signal of methane (S_{max}) as a function of the mole fraction (x_2) in the range $x_2 = 0-0.1$. (Bottom) S_{max} as a function of the square root of the mole fraction.

$$S_{cw}(t) = \left(-\frac{1}{\kappa}\left(\frac{\partial n}{\partial T}\right)_P\right)\left(\frac{\alpha l P}{\pi w_0^2}\right)\left(\frac{1}{1 + t_c/2t}\right)\left(\frac{z'}{1 + z^2/z_0^2}\right)(Y_H)(x_2) \quad (1)$$

where the time-dependent signal ($S_{cw}(t)$) is proportional to the absorbance of the sample ($\alpha x_2 l$) with α being the absorption coefficient, x_2 the mole fraction of the solute, and l the optical path length. The signal magnitude is directly proportional to the negative temperature gradient of the index of refraction ($-dn/dT$) and inversely proportional to the thermal conductivity (κ). The second term in parentheses in eq 1 ($\alpha lP/\pi w_o^2$) is constant because the values of P (20 mW), l (10 cm), and the beam radius at the center of the cell w_o (0.030 cm) remain unchanged for each solution studied.

The third term in parentheses in eq 1 ($1/(1+ t_c/2t)$) is mole-fraction-dependent because the characteristic thermal time constant ($t_c = w_o^2\rho C_P/4\kappa$) is dependent on ρ, κ, and the molar heat capacity (C_P) of the solution ($t_c = 0.30$ s for pure Ar and $t_c = 0.15$ s for pure CH_4). The time (t) is related to the modulation frequency of the pump laser. In our case, with a chopping frequency of 10 Hz the third term reduces the magnitude of the thermal lens signal. Between $x_2 = 0$ and 0.1 the calculated magnitude of third term in parentheses is between 0.25 and 0.27, respectively. To increase this term to the range 0.97−0.99, a chopping frequency of 0.1 Hz would be necessary.

TABLE 1: Thermophysical Properties[a] of Argon and Methane at 93 K

		argon	methane
index of refraction	n	1.2255	1.2929
negative temperature gradient of the index of refraction	dn/dT (K^{-1})	−0.0010	−0.0009
molar density	ρ (mol cm^{-3})	0.035	0.028
thermal conductivity	κ (W m^{-1} K^{-1})	0.116	0.220
coefficient of thermal expansion (vol.)	β (K^{-1})	0.0053	0.0029

[a] From refs 25−27.

The fourth term in parentheses in eq 1 ($z'/(1 + (z/z_o)^2)$) is constant once the values of z, z', and z_o are set. In our experiment the pump laser is focused at the center of the sample cell and the probe laser focus position was set to maximize the resulting signal. The fifth term in parentheses in eq 1 is the heat or energy yield (Y_H). This term, to be considered later, is related to the energy-transfer mechanism from the molecule that absorbs the pump laser to the solution.

Most analytical applications[12] have made use of eq 1 for dual-beam experiments, showing the linear proportionality between S_{max} and the mole fraction x_2 (or concentration) of the solute. Usually the experiments involve very dilute solutions where the laser wavelength is tuned to an electronic transition of the solute with a large absorption coefficient (α). Under these conditions the thermal properties ($-dn/dT$) and κ are associated with properties of the solvent. By exciting a high vibrational overtone, the absorption coefficient of the sample is always very small. In the case of pure liquid CH_4 the reported[16,17] ($\Delta\nu = 6$) C−H peak absorption coefficient is 3×10^{-3} cm^{-1}. This means that in our experiment we are able to study the proportionality presented by eq 1 over a wider range of concentrations (mole fractions) of the solute. In this case the thermal properties of the solution (not the solvent) are the ones to be explored.

4.2. Solution Properties and Thermal Lens Signal. A simple model is proposed to explain the experimental results. It is well known that interactions between CH_4 molecules and Ar atoms in liquid solution are weak.[18] In first approximation, let us consider the CH_4−Ar solutions as ideal and assume that the index of refraction (n) of the solution can be obtained with the Lorentz−Lorenz equation[19,20]

$$\left(\frac{n^2-1}{n^2+2}\right)\frac{1}{\rho} = \left(\frac{n_1^2-1}{n_1^2+2}\right)\frac{x_1}{\rho_1} + \left(\frac{n_2^2-1}{n_2^2+2}\right)\frac{x_2}{\rho_2} \tag{2}$$

Heller[21] used eq 2 to derive the following analytical expression for the index of refraction

$$n = \left(\frac{2A+1}{1-A}\right)^{1/2}$$

$$A = \left[\left(\frac{n_1^2-1}{n_1^2+2}\right)\frac{x_1}{\rho_1} + \left(\frac{n_2^2-1}{n_2^2+2}\right)\frac{x_2}{\rho_2}\right]\rho \tag{3}$$

The density (ρ), the coefficient of thermal expansion (β), and the thermal conductivity (κ) of the solution are given by the following equations[22−24]

$$\rho = \rho_1 + (\rho_2 - \rho_1)x_2 \tag{4}$$

$$\beta = \beta_1 + (\beta_2 - \beta_1)x_2 \tag{5}$$

$$\kappa = \kappa_1 + (\kappa_2 - \kappa_1)x_2 \tag{6}$$

that are also functions of the mole fraction of the solute (x_2). The terms n_1, ρ_1, β_1, and κ_1 refer to the solvent (Ar), and n_2, ρ_2, β_2, and κ_2 refer to CH_4. Table 1 presents numerical values of these properties for Ar and CH_4.

Each experiment was done at a constant mole fraction of solute (x_2). The partial derivative of n (eq 3) with respect to the temperature at constant pressure is

$$\left(\frac{\partial n}{\partial T}\right)_P = \frac{3}{2(2A+1)^{1/2}(1-A)^{3/2}}\left(\frac{\partial A}{\partial T}\right)_P \tag{7}$$

$$\left(\frac{\partial A}{\partial T}\right)_P = A_1x_1 + A_2x_2 \tag{8}$$

$$A_i = \left(\frac{\rho}{\rho_i}\left(\frac{\partial}{\partial T}\left(\frac{n_i^2-1}{n_i^2+2}\right)\right)_P + \left(\frac{n_i^2-1}{n_i^2+2}\right)\left(\frac{\partial}{\partial T}\left(\frac{\rho}{\rho_i}\right)\right)_P\right), \quad i = 1, 2 \tag{9}$$

$$A_i = \frac{\rho}{\rho_i(n_i^2+2)}\left(2n_i\left(\frac{\partial n_i}{\partial T}\right)_P\left(1 - \frac{n_i^2-1}{n_i^2+2}\right) + (n_i^2-1)(\beta - \beta_i)\right) \tag{10}$$

In eq 10 the variation of the density with temperature at constant pressure has been replaced by the product of the density (ρ) and the coefficient of thermal expansion (β) of the solution as well as the corresponding $\beta_i\rho_i$ of Ar or CH_4. The function $g(x_2)$ is defined multiplying eq 7 by $(-1/\kappa)$

$$g(x_2) = -\frac{1}{\kappa}\left(\frac{\partial n}{\partial T}\right)_P = -\frac{3}{2\kappa(2A+1)^{1/2}(1-A)^{3/2}}(A_1x_1 + A_2x_2) \tag{11}$$

This function $g(x_2)$ is the first term in parentheses on the right-hand side of eq 1 and is positive because ($\partial n/\partial T$) is negative. The product function $x_2g(x_2)[1/(1 + t_c/2t)]$ was calculated numerically. Figure 6 (top) shows the result of the calculation as a function of x_2 (solid line). The experimental points are the full circles connected by broken lines. To make the comparison, the calculated and experimental results were both normalized to the S_{max} of pure methane. The calculated results qualitatively simulate the curvature of the experimental results. In Figure 6 (bottom) the experimental and calculated results were normalized to S_{max} at 0.084 mole fraction. This was done to facilitate the comparison in this low concentration region. It is clear that the experimental results are not simulated by the product function that is linear in this region.

4.3. Energy-Transfer Mechanism. The last term that needs to be considered is the quantum yield for nonradiative relaxation of the vibrational excitation energy (Y_H). This term is related to the energy-transfer mechanism from the molecule that absorbs the pump laser to the solution. The ultimate temperature change that occurs in solution is proportional to the relaxation rate of the excited molecule and the efficiency of the energy-transfer mechanism. This is dependent on the nature of the excited state, the concentrations of all species present, the intermediate energy levels available to the molecule, and the properties of the solvent.

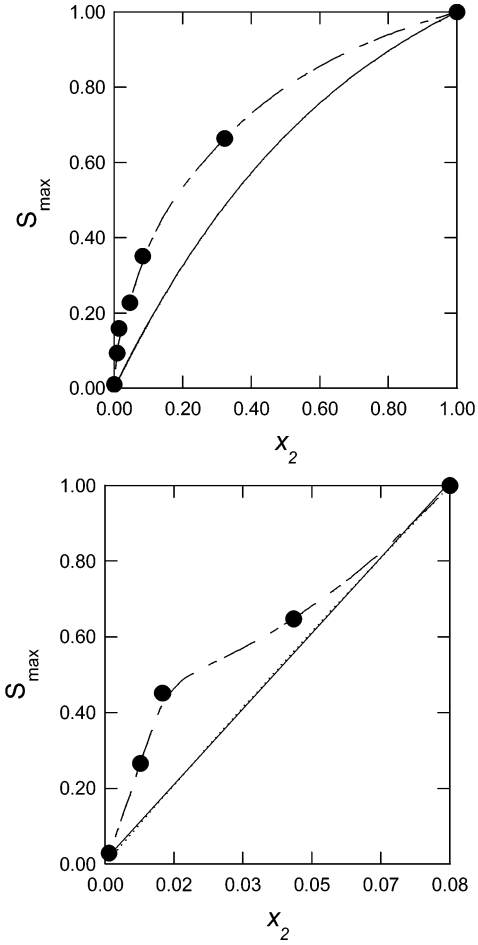

Figure 6. Calculated product function $x_2g(x_2)[1/(1 + t_c/2t)]$ (see text) as a function of the mole fraction (x_2) (solid line). The experimental points are the full circles connected with broken lines. (Top) Calculated and experimental results normalized to the S_{max} of pure methane. (Bottom) Calculated and experimental results normalized to the S_{max} at 0.084 mole fraction. This was done to facilitate the comparison in two concentration regions.

To determine the energy-transfer mechanism for the liquid solution CH_4-Ar a time-resolved experiment needs to be done with a pulsed laser as the excitation source. On the basis of the results, mechanisms of energy transfer could be proposed. In the absence of such a study, some observations can be made with the present measurements. The term Y_H is dependent on the energy-transfer mechanism. Depending on the concentration of methane, different mechanisms could become dominant.

The mechanism of energy transfer for methane below 3000 cm^{-1} has been studied in the gas phase.[28,29] The following equilibration pathway that involves the sequential flow of energy has been proposed: $CH_4(\nu_3) \rightarrow CH_4(\nu_4) \rightarrow CH_4(\nu_2)$.

The pathway for vibrational energy equilibration begins with

$$CH_4(\nu_3) + CH_4 \rightleftharpoons CH_4(2\nu_4) + CH_4;\ \Delta E = -419\ cm^{-1} \quad (12)$$

followed by

$$CH_4(2\nu_4) + CH_4 \rightleftharpoons 2CH_4(\nu_4);\ \Delta E = -5\ cm^{-1} \quad (13)$$

and the equilibrium

$$CH_4(\nu_4) + CH_4 \rightleftharpoons CH_4(\nu_2) + CH_4;\ \Delta E = 227\ cm^{-1} \quad (14)$$

occurring on roughly the same time scale as that for the combined processes of eqs 12 and 13. The experimental evidence indicates that the rise of ν_4 is faster than the fall of ν_3, and this is probably due to equilibrium 14. To test this hypothesis, Weitz and Flynn[29] proposed an experiment at high rare gas pressure. In this case equilibration between ν_4 and ν_2 should be very fast. Step 13 should not be affected because it is a resonant energy-transfer process. The end result is that the rise of ν_4 and fall of ν_3 should become closer in magnitude. The relaxation of ν_3 occurs through infrared emission and energy transfer that ends with levels ν_4 and ν_2. Relaxation of ν_4 is through infrared emission. Relaxation of ν_2 (IR inactive) is through V−R,T processes or through eq 14. In the gas phase at 295 K the V−V equilibration is about 2 orders of magnitude faster than V−R,T transfer.

Time-dependent studies of energy transfer in cryogenic liquid solutions such as M−Ar and $M-N_2$ below 100 K have only been done for excitation of vibrational fundamental and low-energy combination bands and overtones.[30−35] The solute M refers to CH_4, CD_4, CO_2, N_2O, CO, and other small molecules. We are not aware of kinetic studies of energy transfer in cryogenic liquid solutions where high vibrational overtones are excited. In the case of pure liquid N_2 the V−T relaxation time is around 60 s because ΔE is 2326 cm^{-1} and at 77 K, although there are many collisions in the liquid, only a small percentage of the collisions are energetic enough to produce V−T relaxation. For solutions $M-N_2$ the relaxation occurs mainly through V−V energy transfer to the M molecule, followed by V−T relaxation of M. The liquid CH_4-N_2 study of Calaway and Ewing[30] measured the relaxation of excited N_2 but did not follow the IR emission from methane.

If it is assumed that in our study most of the energy of CH_4 ($\upsilon = 6$) ends up in the fundamental (ν_3) and the gas-phase mechanism is adopted, equilibrium 13 could be the key to explain the linear dependence of S_{max} on $(x_2)^{1/2}$. In kinetics, usually the order $^1/_2$ appears as a result of a reaction similar to eq 13. At smaller mole fractions of methane equilibrium reactions 12 and 14 will not be affected if CH_4 is replaced by Ar but equilibrium 13 cannot occur, eliminating any $(x_2)^{1/2}$ dependence.

The sensitivity of the thermal lens technique represents a remarkable improvement compared with our own photoacoustic measurements. Previously[13] we measured the ($\Delta\upsilon = 6$) C−H methane overtone spectrum in liquid argon for a solution of 0.1 mole fraction. The detection limit was increased 100 times using the thermal lens technique. Almost identical considerations enhance the photoacoustic signal and the thermal lens signal, but our comparison is with the cw acoustic method. The cw photoacoustic technique that we used in the past requires finding a resonant modulation frequency (kHz) that depends on the radius and length of the cell as well as the speed of sound in the liquid solvent. It is not always possible to find the strongest resonance in the range of frequencies that the lock-in amplifier permits. If a pulsed laser is used with the acoustic technique, this limitation does not apply. The cw thermal lens technique is more flexible than the cw acoustic technique because if both techniques use the same pump laser power, it is possible to increase the sensitivity of the thermal lens technique by decreasing the size of the pinhole or decreasing the modulation frequency. Use of argon as the solvent enhances the thermal lens signal because the excited sample molecule can only transfer energy to translational motion of the solvent.

5. Conclusion

A dual-beam thermal lens technique has been used to obtain the absorption spectrum of the ($\Delta\upsilon = 6$) C−H stretch of liquid

methane and methane in liquid argon solutions. The lowest concentration detected was 1×10^{-3} (mole fraction) of CH_4 in liquid Ar. Thermophysical properties of the solution qualitatively explain the magnitude of the signal as a function of the mole fraction of methane but not the details at mole fractions below 0.1. The gas-phase mechanism of energy transfer[28] from vibrationally excited methane could in principle be used to explain qualitatively the magnitude of the signal as a function of the mole fraction and its linearity with the square root of the mole fraction. A time-dependent study is needed to find the mechanism of energy transfer in the liquid. We are currently doing more experiments in the region $x_2 = 0.01-0.1$ to determine if the present results are general or if it is dependent on the particular conditions of laser power, temperature, and modulation frequency under which the results were obtained. Detection of the overtone spectrum of methane at $x_2 = 1 \times 10^{-3}$ indicates an absorption (αx_2) of approximately 3×10^{-6} cm^{-1} or an absorbance ($\alpha x_2 l$) of 3×10^{-5}.

Acknowledgment. This work was supported by the Robert A. Welch Foundation under Grant No AA-1173. This study was supported in part by funds from the Quantum Optics Initiative funded by the ONR, Texas A&M, and the Vice Provost for Research at Baylor University. Partial support from the Baylor University Research Committee is also acknowledged.

References and Notes

(1) Long, M. E.; Swofford, R. L.; Albrecht, A. C. *Science* **1976**, *191*, 183.
(2) Swofford, R. L.; Long, M. E.; Albrecht, A. C. *J. Chem. Phys.* **1976**, *65*, 179.
(3) Swofford, R. L.; Long, M. E.; Burberry, M. S.; Albrecht, A. C. *J. Chem. Phys.* **1977**, *66*, 664.
(4) Fang, H. L.; Swofford, R. L. *J. Chem. Phys.* **1980**, *72*, 6382.
(5) Fang, H. L.; Swofford, R. L. *J. Chem. Phys.* **1980**, *73*, 2607.
(6) Gordon, J. P.; Leite, R. C. C.; Moore, R. S.; Porto, S. P. S.; Whinnery, J. R. *J. Appl. Phys.* **1965**, *36*, 3.
(7) Hu, C.; Whinnery, J. R. *Appl. Opt.* **1973**, *12*, 72.
(8) Whinnery, J. R. *Acc. Chem. Res.* **1974**, *7*, 225.
(9) Imasaka, T.; Miyaishi, K.; Ishibashi, N. *Anal. Chim. Acta* **1980**, *115*, 407.
(10) Harris, J. M.; Dovichi, N. J. *Anal. Chem.* **1980**, *52*, 695A.
(11) Fang, H. L.; Swofford, R. L. *Ultrasensitive Laser Spectroscopy*; Kliger, D. S., Ed.; Academic Press: New York, 1983; p 176.
(12) Bialkowski, S. E. *Photothermal Spectroscopy Methods for Chemical Analysis*; Wiley: New York, 1996; p 390.
(13) Blunt, V. M.; Cedeño, D. L.; Manzanares, C. E. *Mol. Phys.* **1997**, *91*, 3.
(14) Manzanares, C. E.; Mina-Camilde, N.; Brock, A.; Peng, J.; Blunt, V. M. *Rev. Sci. Instrum.* **1995**, *66*, 2644.
(15) Tam, A. C. *Rev. Modern Phys.* **1986**, *58*, 381.
(16) Patel, C. K. N.; Nelson, E. T.; Kerl, R. J. *Nature* **1980**, *286*, 368.
(17) Ramaprasad, K. R.; Caldwell, J.; McClure, D. S. *Icarus* **1978**, *35*, 400.
(18) Bulanin, M. O. *J. Mol. Struct.* **1973**, *19*, 59.
(19) Lorentz, H. A. *Wied. Ann.* **1880**, *9*, 641.
(20) Lorenz, L. *Wied. Ann.* **1880**, *11*, 70.
(21) Heller, W. *J. Phys. Chem.* **1965**, *69*, 1123.
(22) Heyes, D. M. *J. Chem. Phys.* **1992**, *96*, 2217.
(23) Mikhailenko, S. A.; Dudar, V. G.; Derkach, V. N.; Zozulya, V. N. *Sov. J. Low Temp. Phys.* **1977**, *3*, 331.
(24) Mikhailenko, S. A.; Dudar, V. G.; Derkach, V. N. *Sov. J. Low Temp. Phys.* **1978**, *4*, 205.
(25) *CRC Handbook of Chemistry and Physics*, 64th ed.; Weast, R. C., Ed.; CRC: Cleveland, OH, 1983; p E10.
(26) Jain, S. C.; Nanda, V. S. *J. Phys. C: Solid State Phys.* **1971**, *4*, 3045.
(27) Younglove, B. A.; Ely, J. F. *J. Phys. Chem. Ref. Data* **1987**, *16*, 577.
(28) Hess, P.; Moore, C. B. *J. Chem. Phys.* **1976**, *65*, 2339.
(29) Weitz, E.; Flynn, G. *Photoselective Chemistry, Part 2*; Jortner, J., Levine, R. D., Rice, S. A., Eds.; John Wiley and Sons: New York, 1981; p 185.
(30) Calaway, W. F.; Ewing, G. E. *J. Chem. Phys.* **1975**, *63*, 2842.
(31) Manzanares, C. E.; Ewing, G. E. *J. Chem. Phys.* **1978**, *69*, 1418.
(32) Manzanares, C. E.; Ewing, G. E. *J. Chem. Phys.* **1978**, *69*, 2803.
(33) Brueck, S. R. J.; Osgood, R. M. *Chem. Phys. Lett.* **1976**, *39*, 568.
(34) Brueck, S. R. J.; Deutsch, T. F.; Osgood, R. M. *Chem. Phys. Lett.* **1977**, *51*, 339.
(35) Brueck, S. R. J.; Osgood, R. M. *J. Chem. Phys.* **1978**, *68*, 4941.